

## Ibn Al-Haitham Journal for Pure and Applied Sciences

Journal homepage: jih.uobaghdad.edu.iq PISSN: 1609-4042, EISSN: 2521-3407 IHJPAS. 2025, 38(4)



# Synthesis, Characterization and Photocatalytic Activity of ZrO<sub>2</sub> Nanoparticles using Mint Extract

Noor Mohammed Jasam<sup>1,2</sup> ▶ Lekaa K. Abdul Karem<sup>2\*</sup> ▶, and Ahmed M. Khalil<sup>3</sup>

<sup>1,2</sup>Departments of Chemistry, College of Education for Pure Science (Ibn Al-Haitham), University of Baghdad, Baghdad, Iraq.

<sup>3</sup>Photochemistry Department, National Research Centre, 33 El-Bohouth St, Dokki, Giza, 12622, Egypt. \*Corresponding author.

Received: 1 May 2025 Accepted: 17 July 2025 Published: 20 October 2025

doi.org/10.30526/38.4.4160

#### **Abstract**

This work describes a green synthesis route for zirconium oxide nanoparticles (ZrO<sub>2</sub> NPs) by using Zr sulfate and mint extract. This method is distinguished from other processes (physical and chemical) by its simplicity, cost-effectiveness, and low potential risks during preparation. Multiple techniques have been used to characterize and analyze ZrO<sub>2</sub> NPs, including Fourier transform infrared and ultraviolet visible spectra, crystal size calculation by X-ray diffraction, scanning electron and atomic force microscopes, energy-dispersive X-ray, and Zeta potential. Kinetic stability of the ZrO<sub>2</sub> NPs system, as indicated by the Zeta potential of -25.8 mV, suggests a long-term persistence and high surface charge. Finally, photo-catalytic activities of zirconium oxide NPs were examined using methylene blue dye. The results showed that the dye's degradation efficiency under light irradiation was 96.88%, demonstrating its significant photo-catalytic potential. The x-ray diffraction analysis of the crystal size of ZrO<sub>2</sub> NPs, using Debye Scherrer's equation, yielded a value of 18.78 nm. The prepared ZrO<sub>2</sub> NPs were tetragonal.

**Keywords:** Microscopy, Photo-catalytic activities, Transmission electron, X-ray diffraction, Zirconium oxide nanoparticles.

#### 1. Introduction

Nanotechnology is a multidisciplinary field of interest, attracting researchers from areas such as physics, chemistry, biology, engineering, medicine, and materials science due to its potential to design nanoparticles (NPs) with controlled shapes and dimensions (1,2). While several approaches exist for NPs synthesis, environmentally friendly, cost-effective, and sustainable "green synthesis" techniques are increasingly preferred over conventional physical and chemical methods. Traditional chemical methods often involve high costs and hazardous reagents (3,4), and typically require additional stabilizers or additives to maintain particle stability. These processes may also utilize non-biodegradable solvents and demand extreme conditions such as high temperatures and pressures (5-7). On the contrary, biological or green biosynthesis leverages natural resources—such as bacteria, fungi, algae, and especially plant extracts—to generate NPs without resorting to toxic chemicals. Among these

biological sources, plant extracts stand out for their simplicity, low environmental impact, and cost-effectiveness, as well as for yielding stable NPs (8-11). Plant-derived phytochemicals play a significant role as natural reducing and capping agents during synthesis. Examples include neem (Azadirachta indica), hibiscus (Hibiscus rosa-sinensis), and Indian gooseberry (Emblica officinalis), which have demonstrated effectiveness in producing metal oxide NPs. Spinach, in particular, is a valuable green source due to its rich composition of vitamins (A, C, E, K), folic and oxalic acids, and essential minerals like Mn, Mg, Ca, P, Fe, Zn, Cu, Se, and K. Moreover, it contains important phytochemicals such as carotenoids (β-carotene, lutein, zeaxanthin), chlorophyll, glutathione, α-lipoic acid, betaine, and various phenolic compounds (12-15), all of which contribute to its antioxidant properties and facilitate nanoparticle formation. Previous research has successfully synthesized zirconium oxide (ZrO<sub>2</sub> NPs) using biological agents, including Euclea natalensis (16), the fungus Fusarium solani (17), various plant leaves (18), Curcuma longa (19), pomegranate peel (20), and cinnamon (21). These studies have explored diverse applications ranging from adsorption and thermodynamic analysis to evaluating the biological activity, toxicity, and antioxidant properties of ZrO<sub>2</sub> NPs (22). For instance, synthesis using thyme extract at pH 12 yielded ZrO NPs with an average crystallite size of 18.7 nm, as determined by the Debye-Scherrer equation (23). This study aims to characterize the ZrO<sub>2</sub> NPs prepared from mint plant extract using various methods, such as X-ray diffraction (XRD), field emission scanning electron microscopy and electron density (FESEM-EDS), transmission electron microscope (TEM), and zeta potential. In addition to analyzing the infrared and ultraviolet spectra of the NPs, the photo-catalytic activity (PCA) was utilized as a practical application using methyl blue dye, yielding favorable results.

#### 2. Materials and Methods

The acquired specimens were sourced from a local location and utilized ZrSO<sub>4</sub> (purchased from Merck, Germany), NaOH (obtained from Sigma Aldrich, America), and deionized water (DW) sourced from local markets.

#### 2.1. Preparation of mint extract and ZrO<sub>2</sub> NPs

The same method described in (24) was used. Fresh Mint was gathered and washed by DW to remove any existing impurities, dried, and then blended into a fine, uniform powder. Then, 20 g of this powdered Mint was mixed with 200 mL of DW, and then heated to 70-80 °C for 30 minutes while stirring. The mixture was then filtered and stored in the refrigerator for later use. To synthesize ZrO<sub>2</sub> NPs using the biosynthesis method, 100 mL of Mint extract was carefully added, drop by drop (1 drop per second), to 100 mL of 0.1 M Zr(SO<sub>4</sub>)<sub>2</sub>. The solution was stirred for 30 minutes, and then a sodium hydroxide solution (made by dissolving 2 g of NaOH in 50 mL of DW) was added gradually until the pH reached 12. This process led to the formation of a dark green precipitate, which was purified by washing with deionized water using centrifugation and decantation. The purified precipitate was then dried in an oven and calcined at 800°C for 3 hours, ultimately producing a yellowish powder of ZrO<sub>2</sub> NPs.

#### 2.2. The photo-catalytic activity

The PCA of ZrO<sub>2</sub> NPs was evaluated using an organic dye; a 10 mg/L concentration of MB was taken as a model pollutant. The stock solution of MB was diluted with deionized water to prepare the working solution at a final concentration of 5 mg/L. A specific amount of ZrO<sub>2</sub> NPs (0.5 g/L) was weighed and dispersed into the pollutant solution. To ensure homogeneity, sterilize the mixture with ultrasound for 30 minutes, then transfer the suspension to a quartz

photo reactor. The reactor was equipped with a high-efficiency light source, a xenon lamp with a power output of 300 W, to provide the required irradiation. Before illumination, the suspension was stirred in complete darkness for 30 minutes to establish adsorption-desorption equilibrium between the pollutant molecules and the catalyst surface. Following this equilibrium phase, the light source was activated, and the photo-catalytic reaction was initiated, with the suspension exposed to light for 120 minutes. During the reaction, aliquots of the solution were withdrawn at regular time intervals of 20 minutes. Each aliquot was filtered using a syringe filter with a pore size of 0.22 µm to remove residual NPs (24). The residual concentration of the pollutant in the filtered aliquots was measured with a UV spectrophotometer at 664 nm, the characteristic wavelength of MB. **Equation 1** below shows the calculation of the photo-catalytic decomposition efficiency.

Degradation Efficiency (%) = 
$$\frac{C_0 - Ct}{C_0} \times 100$$
 (1)

Where  $C_0$  is the initial concentration of the pollutant, and Ct is the concentration at time t. To ensure the accuracy and reproducibility of the results, all experiments were performed in triplicate, and the average values were reported. Control experiments were also conducted to verify the photo-catalytic nature of the degradation process, including tests without the catalyst (light only) and tests in the dark (catalyst only). These control studies confirmed that the observed degradation was solely attributable to the photo-catalytic activity of the  $ZrO_2$  NPs. The results demonstrated that the  $ZrO_2$  NPs exhibit excellent photo-catalytic efficiency, achieving significant pollutant degradation within the reaction time. This highlights their potential as effective photo catalysts for environmental remediation applications (24).

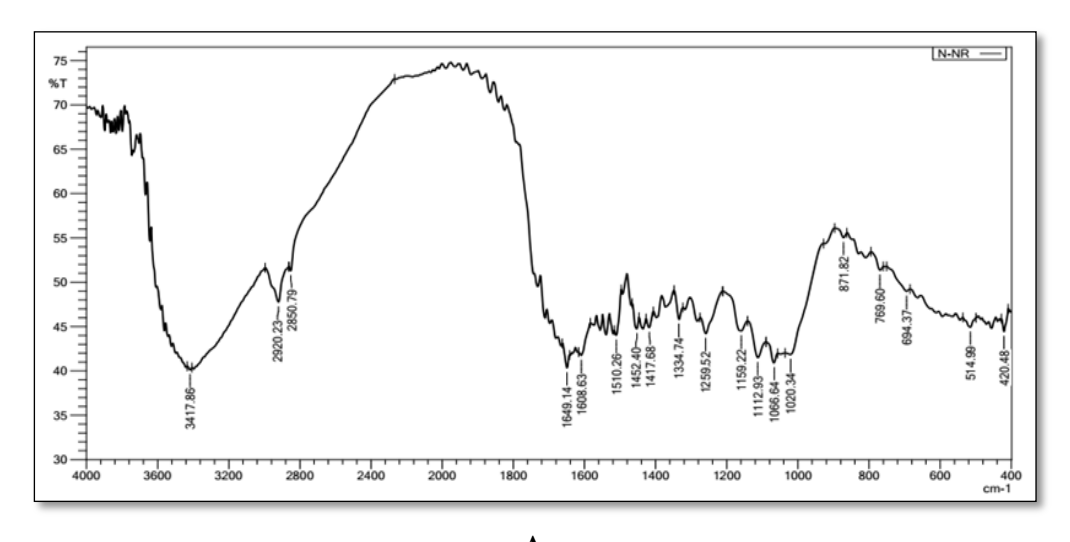
#### 2.3. Product characterisation

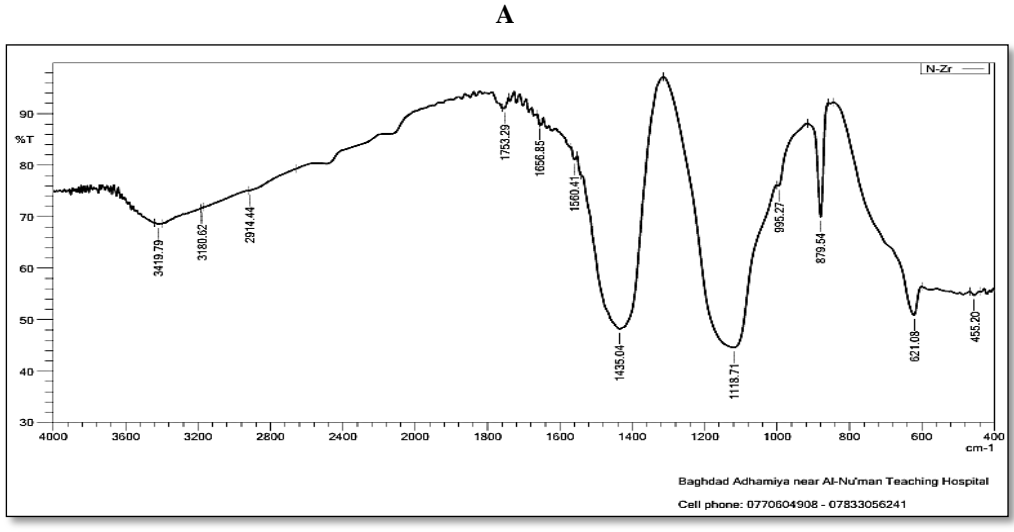
The compounds were created and identified using various spectroscopic and microscopic techniques and equipment, including a magnetic stirrer, an electric oven of type PC21-A, Batec, an electric centrifuge of type PLC (80-1), and a sensitive electronic balance (AS 220C1) was used for precise measurements. FT-IR spectrum was measured with a Shimadzu 1800 (Japan) in the range of 400-4000 cm<sup>-1</sup>. UV-Visible spectroscopy was conducted with a UV-Vis spectrophotometer, and the FTIR and UV-Visible were tested at the University of Baghdad. XRD analysis was performed using a Phillips PW1730 (Netherlands). The structural composition and elemental content were measured by energy-dispersive X-ray spectrometry (EDX) and FESEM-EDS model MIRA II (Czech Republic). Additionally, a TEM model EM10C-100Kv (Zeiss, Germany) was used for further examination. XRD, EDX, TEM, and FESEM-EDS were tested at the University of Kashan/ Islamic Republic of Iran. The Zeta potential was tested at the University of Technology, Baghdad.

#### 3. Results

#### 3.1. Data analysis of FT-IR

The FTIR of mint leaf extract, **Figure 1A**, shows absorption bands at 3417, 1608, 1417, 1259, and 1020 cm<sup>-1</sup>. The results of infrared spectroscopy of the obtained ZrO<sub>2</sub> NPs synthesized using Mint extract are shown in **Figure 1B**; many bands are shown at 3419 cm<sup>-1</sup>.





В

Figure 1. Data analysis of the spectrum, A- Mint leaves, B- ZrO<sub>2</sub> NPs.

## 3.2.Data analysis of UV-Visible

The UV-vis spectrum of ZrO<sub>2</sub> NPs in 10<sup>-3</sup>M concentration and DMSO as a solvent in **Figure** 2, displays peaks of absorption at (234 and 370) nm.

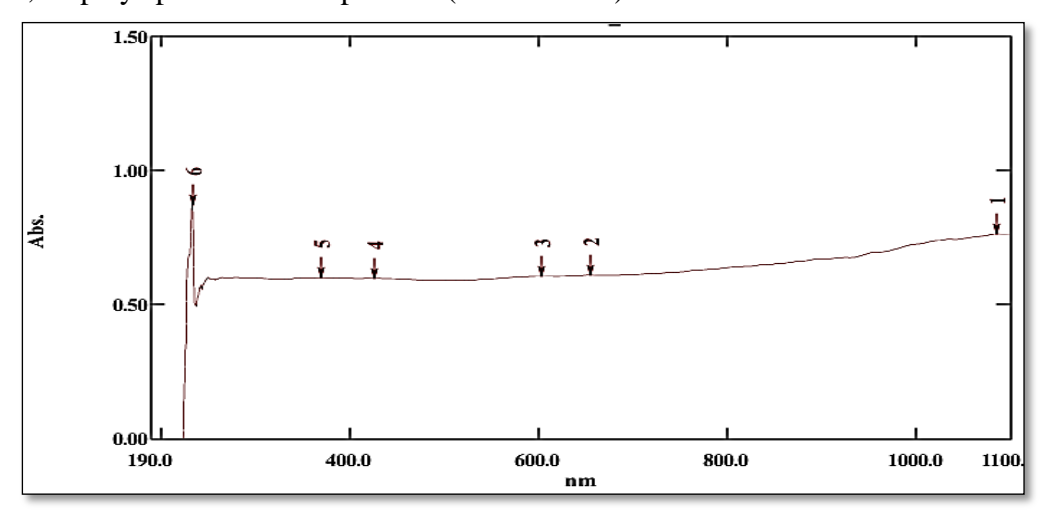


Figure 2. Data analysis of the UV- visible spectrum of ZrO<sub>2</sub> NPs.

## 3.3. Data analysis of X-RD and EDX

Based on the XRD study presented in **Table 1** and **Figure 3**, it has been determined that the crystal planes of ZrO<sub>2</sub> NPs, which are consistent with miller indices, 101, 103, 202, 321 and

224 have been assigned to several XRD position peaks at (°2Th.) values (27.935, 29.618, 31.645, 49.949 and 59.550) respectively, closely match the conventional diffraction peaks of JCPDS card number (No. 24-0734).

**Table 1.** Data analysis of XRD of ZrO<sub>2</sub> NPs.

Pos. [°2Th.]	hkl	FWHM (deg)	2 theta (Rad.)	FWHM (Rad.)	P.s (nm)	Medium size
27.9357	101	0.39	0.255001	0.002	21.74	
29.6187	103	0.49	0.285396	0.003	17.46	
31.6458	202	0.30	0.317627	0.004	29.24	
49.9492	321	0.69	0.512779	0.008	13.30	18.78nm
59.5509	224	0.79	0.525129	0.002	12.15	

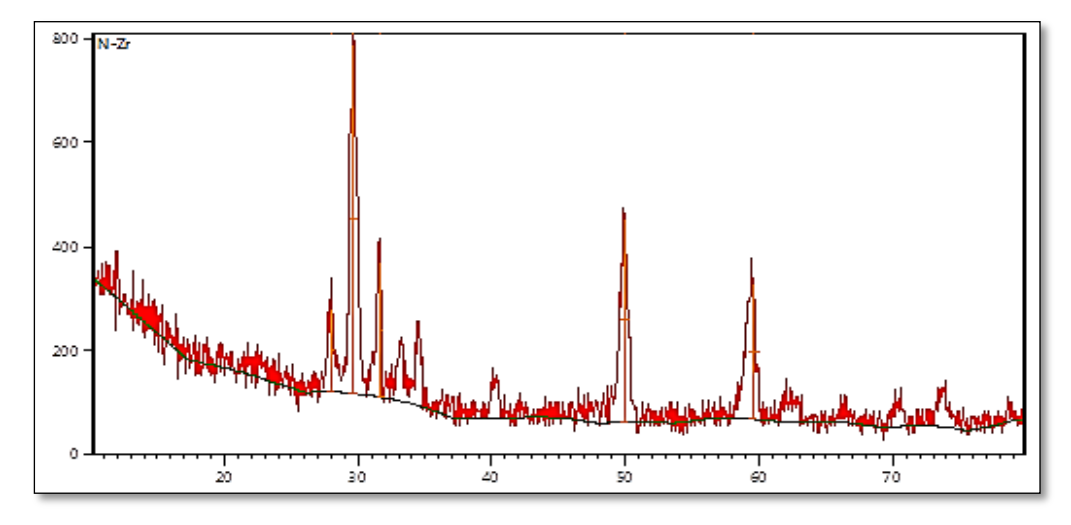


Figure 3. The XRD analysis of ZrO<sub>2</sub> NPs.

The EDX was used to analyze the percentage (%) of elements in the ZrO<sub>2</sub> NPs, as shown in **Figure 4**. The element percentages showed 60% for Zr and 40% for oxygen.

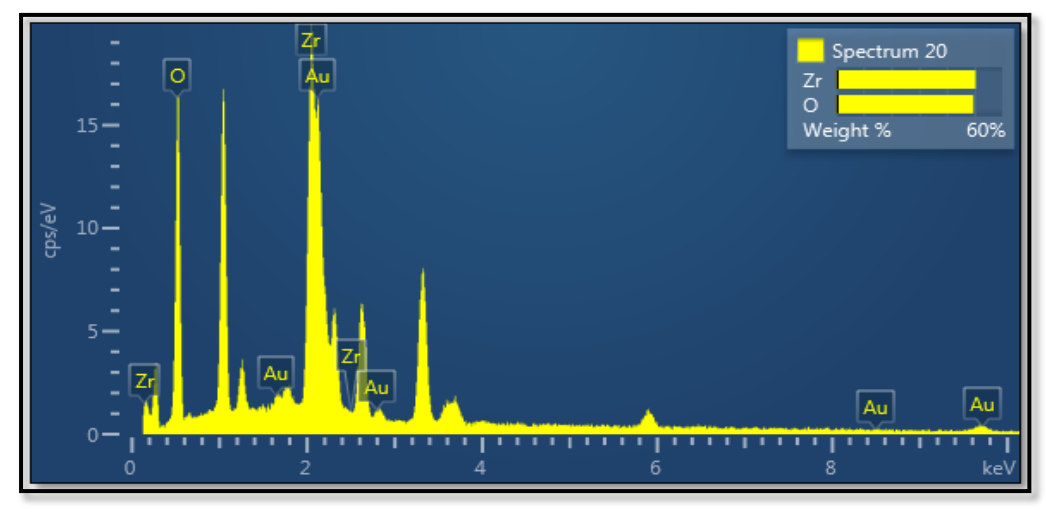
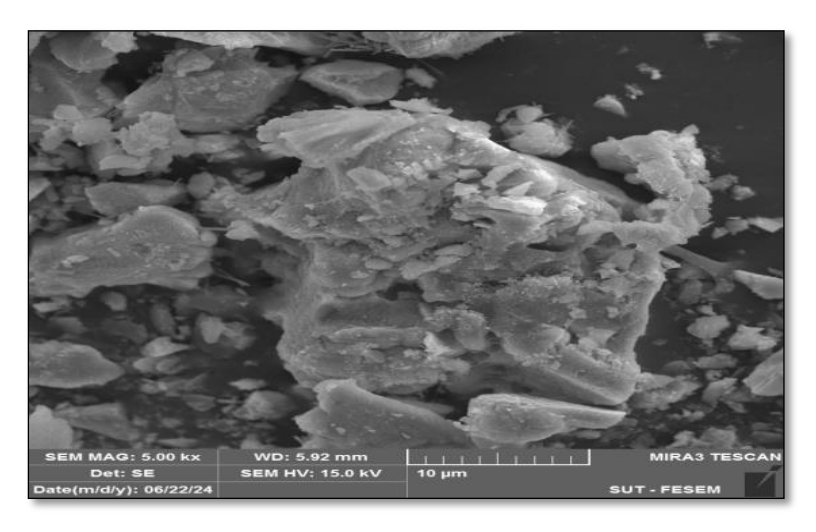


Figure 4. The EDX of ZrO<sub>2</sub> NPs.

## 3.4. Data analysis of SEM and TEM

The morphology and structure of the nanomaterial were determined by scanning electron microscopy. SEM images in **Figure 5** confirm the precise formation of ZrO<sub>2</sub> NPs in small clusters. The TEM image reveals that the sample consists of spherical and irregular NPs structures within a (15-50) nm range with a zero-dimensional morphology as seen in **Figure 6**.



**Figure 5.** The Images of SME for ZrO<sub>2</sub> NPs.

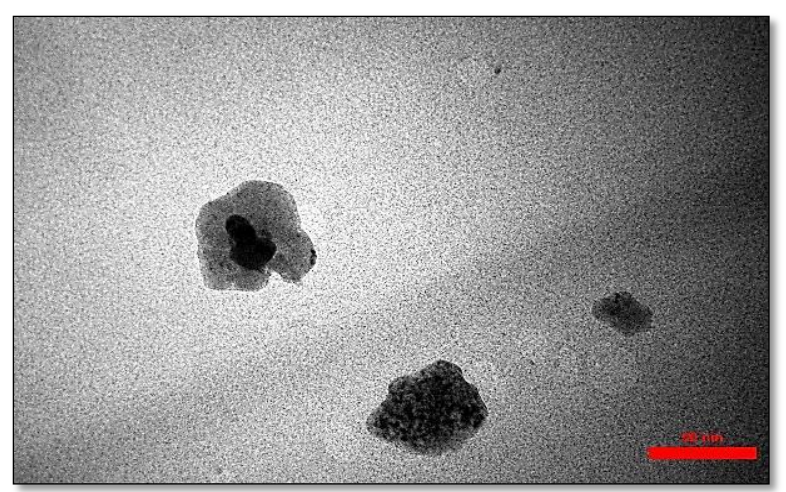


Figure 6. The images of TME for ZrO<sub>2</sub> NPs.

## 3.5. Zeta potential of ZrO<sub>2</sub> NPs

The zeta potential of  $ZrO_2$  NPs synthesized from Mint plant extract was -25.8 mV, as shown in **Figure 7**.

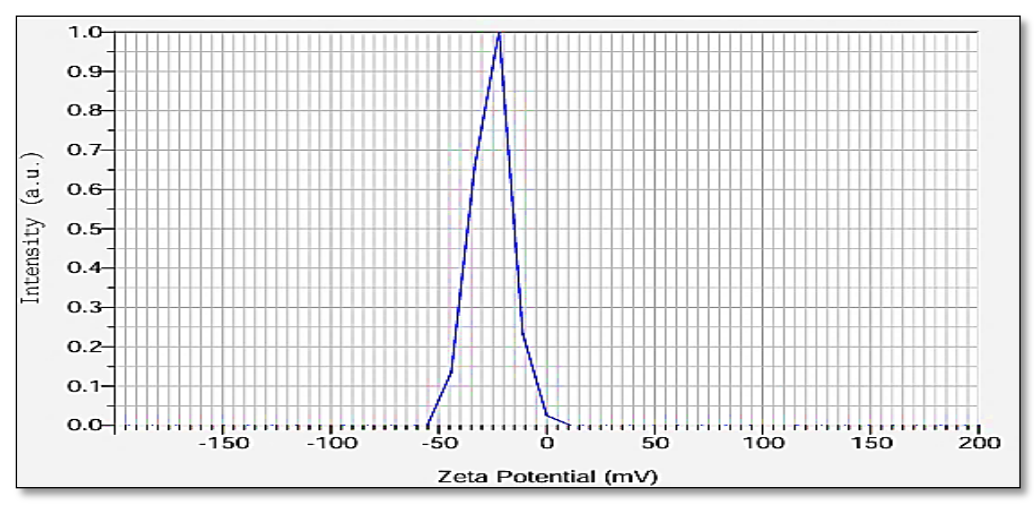
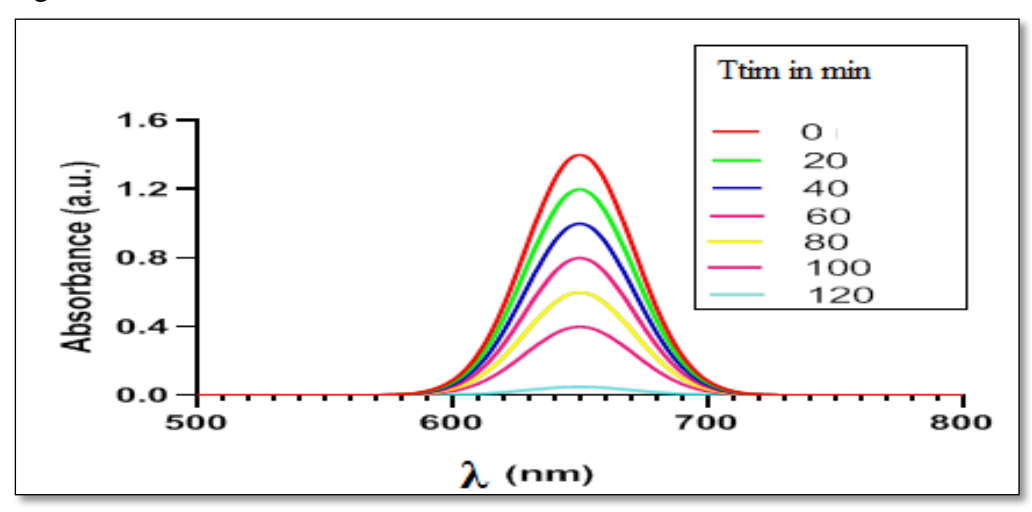


Figure 7. The images of Zeta potential of ZrO<sub>2</sub> NPs.

#### 3.6. Photo-catalytic degradation of MB

The photo-catalytic activity of ZrO<sub>2</sub> NPs was evaluated by light irradiation for the degradation of MB dye. The absorption spectra, measured at different time intervals, exhibited a distinct peak at 664 nm, corresponding to the characteristic absorption of MB. Initially, at time 0 minutes, the absorption was at its maximum (~1.6 absorbance units), reflecting the full concentration of MB in the solution. Over time, a consistent decrease in absorption was observed at intervals of (20, 40, 60, 80, 100, and 120) minutes as shown in **Figure 8**. The gradual degradation of MB molecules, by the end of the experiment (120 minutes), the absorption approached nearly zero, signifying that most of the MB had been degraded.



**Figure 8.** The UV-VIS spectra of MB catalyzed by ZrO<sub>2</sub>NPs.

#### 4. Discussion

#### 4.1. The FTIR spectra

In FTIR, the broad band at 3417 cm<sup>-1</sup> could be attributed to the presence of the hydroxyl functional groups of alcohols and phenolic compounds that may exist in plant extracts. The sharp peak located at 1597 cm<sup>-1</sup> is related to the presence of carbonyl-containing compounds, which may be involved in the bio-reduction of the Zr ion. The peaks at 1403–1279 cm<sup>-1</sup> arise from the C–N stretching mode of aromatic amine groups. The marked peak at 1055 cm<sup>-1</sup> can also be related to the stretching vibration of the C–OH bond from proteins in the plant extract.

## 4.2. The Uv-visible spectrum

The UV-visible spectrum of  $ZrO_2$  NPs shows many peaks at (234 and 370) nm and 400 nm attributed to the transition of holes between Zr and O, indicating a distinctive feature of the biosynthesis process. The absorption peaks above 400 nm are attributed to the d–d transitions of Zr ions in  $ZrO_2$  NPs. The energy gap of  $ZrO_2$  NPs was calculated from the equation: Eg=  $1240/\lambda$ , which is to be (5.29 and 3.35) eV (24).

## 4.3. The XRD pattern and EDX

The observed peaks in **Figure 3** and **Table 1** correspond to the crystallographic planes (hkl) of the prepared ZrO<sub>2</sub> NPs, which were tetragonal crystalline phases as well as monoclinic ones (14). The sizes of the ZrO<sub>2</sub> NPs were determined using the Debye-Scherrer equation, as shown in **Equation 2**, revealing an average size of 18.78 nm.

$$D = \frac{0.9 \,\lambda}{\beta \cos \theta} \tag{2}$$

Where D: the average crystalline size;  $\lambda$ : X-ray wavelength (1.5406 Å) of the copper target;  $\beta$ : maximum width at mid-intensity (FWHM) and converted from degrees to radius; K: shape

factor or shape factor, which is about 0.9-0.94; and  $\theta$ : diffraction angle (24). The XRD pattern shows extra pointless peaks. This may be due to the formation of the crystalline bioorganic compounds and metalloproteins that are present in the extracts (25,26).

EDX was used to analyze the percentage (%) of elements in the ZrO<sub>2</sub> NPs, and the results obtained from this analysis revealed a characteristic peak associated with the % element composition (Zr and O), which corresponds to the exact composition of the sample under study, as shown in **Figure 4**.

## 4.4. The SEM and TEM analyses

The SEM analysis revealed an approximately spherical shape with a rough surface due to the presence of a limited amount of morphology ZrO<sub>2</sub> NPs with nanostructured morphology. This can be seen from the shapes of the SEM images in **Figure 5**, which confirms the precise formation of ZrO<sub>2</sub> NPs formed in small clusters (27). The TEM image reveals that the sample consists of spherical and irregular NPs structures within a (15-50) nm range with a zero-dimensional morphology. This characteristic is highly desirable in surface chemistry, as it enhances the reactivity and stability of nanomaterials. The spherical morphology (confirmed by TEM) enhances the surface-area-to-volume ratio. The well-defined spherical shape suggests uniform particle distribution, which can improve the material's performance in various applications, as seen in **Figure 6**.

## 4.5. Zeta potential

The zeta potential of the synthesized ZrO<sub>2</sub> NPs was -25.8 mV, indicating that the kinetic stability of the ZrO<sub>2</sub> NPs system would persist for a long time due to its high surface charge, and thus can be maintained in suspended form in solution (28).

## 4.6. Photo-catalytic degradation

This degradation is attributed to the photo-catalytic activity of ZrO<sub>2</sub> NPs, which, under light irradiation, produces reactive oxygen species such as (O<sub>2</sub><sup>-•</sup> and •OH) (28). These reactive species attack MB molecules, leading to the breakdown of their chromophoric structure and conversion into harmless byproducts like (CO<sub>2</sub> and H<sub>2</sub>O) (29). The degradation process follows first-order kinetics, where the reaction rate is proportional to the concentration of MB. The degradation efficiency was calculated using the following **Equation 3**:

Degradation efficiency 
$$\% = \frac{A_0 - At}{A_0} \times 100$$
 (3)

Where  $A_{\circ}$  (the initial absorbance) and  $A_t$  (remaining absorbance) are at the wavelength of 664 nm, respectively, using the values extracted from the spectra ( $A_0$ = 1.6 and  $A_t$ = 0.05) at 120 minutes (30), the efficiency was determined to be approximately 96.88%. This high degradation efficiency highlights the remarkable photo-catalytic performance of  $ZrO_2$  NPs, making them a promising material for environmental pollution treatment. Their ability to achieve near-complete degradation of MB within 120 minutes demonstrates their potential for use in wastewater treatment systems. Future studies could focus on optimizing experimental parameters, such as catalyst dosage and light intensity, as well as exploring the reusability and long-term stability of  $ZrO_2$  NPs for large-scale applications (31-33).

## 5. Conclusion

This study describes the eco-friendly synthesis of ZrO<sub>2</sub> NPs using Mint plant extract, which is both efficient and environmentally friendly. FTIR and UV-Vis spectroscopy were used to diagnose the ZrO<sub>2</sub> NPs, which exhibited limited morphology and some deviations due to the presence of large sizes. The SEM technique was used to provide information about the surface morphology and composition of the samples. SEM results showed that the particle size of the ZrO<sub>2</sub> NPs was formed in small clusters. The average crystal size of the ZrO<sub>2</sub> NPs

was 18.78 nm, as confirmed by the XRD and EDX analysis, which showed 60% Zr and 40% O<sub>2</sub>. Zeta potential was -25.8 mV, due to the kinetic stability of ZrO<sub>2</sub> NPs. Photo-catalytic tests showed about 96.88% degradation efficiency of MB dye under light irradiation, emphasizing their essential photo-catalytic potential. The particles are small and spherical.

## Acknowledgment

The authors thank the Department of Chemistry, College of Education for Pure Science (Ibn Al-Haitham) for their support in completing this research.

#### **Conflict of Interest**

The authors declare that they have no conflicts of interest.

## **Funding**

None.

#### **Ethical Clearance**

This study was approved by the University of Baghdad, College of Education for Pure Science (Ibn Al-Haitham).

#### References

- 1. Ahmed KA, Huang K. Formation of Mn<sub>3</sub>O<sub>4</sub> nanobelts through the solvothermal process and their photocatalytic property. Arab J Chem. 2019; 12(3):429-439. https://doi.org/10.1016/j.arabjc.2014.08.014.
- Bello A, Fashedemi OO, Lekitima JN, Fabiane M, Dodoo-Arhin D, Ozoemena KI, Gogotsi Y, Charlie Johnson AT, Manyala N. High-performance symmetric electrochemical capacitor based on graphene foam and nanostructured manganese oxide. AIP Advances. 2013; 3(8):082118. https://doi.org/10.1063/1.4819270.
- 3. Hafez AA, Naserzadeh P, Ashtari K, Mortazavian AM, Salimi A. Protection of manganese oxide nanoparticles-induced liver and kidney damage by vitamin D. RTP. 2018; 98:240-244. <a href="https://doi.org/10.1016/j.yrtph.2018.08.005">https://doi.org/10.1016/j.yrtph.2018.08.005</a>.
- 4. Abduljabar MA, Merza SH. Graphene oxide decorated with nickel cobaltite nanoparticles as an adsorbent for cationic methyl green dye: Kinetic, isotherm, and thermodynamic studies. Baghdad Sci J. 2024; 21(9):2853. <a href="https://doi.org/10.21123/bsj.2024.8742">https://doi.org/10.21123/bsj.2024.8742</a>.
- 5. Ahmad KS, Yaqoob S, Gul MM. Dynamic green synthesis of iron oxide and manganese oxide nanoparticles and their cogent antimicrobial, environmental and electrical applications. Rev Inorg Chem. 2022; 42(3):239-263. https://doi.org/10.1515/revic-2021-0033.
- 6. Perachiselvi M, Bagavathy MS, Samraj JJ, Pushpalaksmi E, Annadurai G. Synthesis and characterization of Mn<sub>3</sub>O<sub>4</sub> nanoparticles for biological studies. Appl Ecol Environ Sci. 2020; 8(5): 273-277. https://doi.org/10.12691/aees-8-5-13.
- 7. Fatin A. Al-jubouri, Basim I. Al-Abdaly. Anti-oxidant and anti-microbial activities of [ZnO: CoO/Eugenol] and [ZnO:Fe<sub>2</sub>O<sub>3</sub>/Eugenol] nanocomposites. IHJPAS. 2024; 37(1):251-64. <a href="https://jih.uobaghdad.edu.iq/index.php/j/article/view/3233">https://jih.uobaghdad.edu.iq/index.php/j/article/view/3233</a>.
- 8. Fernandes C, Benfeito S, Fonseca A, Oliveira C, Garrido J, Garrido EM, Borges F. Photodamage and photoprotection: toward safety and sustainability through nanotechnology solutions. In book: Nanotechnology in the agri-food industry (Muti-Volume SET I-X) Edition: 1<sup>st</sup> Publisher: Elsevier Editors: Alexandru Grumezescu, Ecaterina Andronescu. 2017; 527-565. https://doi.org/10.1016/B978-0-12-804303-5.00015-8.
- 9. Frewer LJ, Gupta N, George S, Fischer AR, Giles EL, Coles D. Consumer attitudes towards nanotechnologies applied to food production. TIFS. 2014; 40(2):211-225. <a href="https://doi.org/10.1016/j.tifs.2014.06.005">https://doi.org/10.1016/j.tifs.2014.06.005</a>.

- 10.Nande A, Raut S, Michalska-Domanska M, Dhoble SJ. Green synthesis of nanomaterials using plant extract: a review. Curr Pharm Biotechnol. 2021; 22(13):1794-1811. https://doi.org/10.2174/1389201021666201117121452.
- 11.Sukhdev A, Challa M, Narayani L, Manjunatha AS, Deepthi PR, Angadi JV, Kumar PM, Pasha M. Synthesis, phase transformation, and morphology of hausmannite Mn<sub>3</sub>O<sub>4</sub> nanoparticles: Photocatalytic and antibacterial investigations. Heliyon. 2020; 6(1):1-18. <a href="https://doi.org/10.1016/j.heliyon.2020.e03245">https://doi.org/10.1016/j.heliyon.2020.e03245</a>.
- 12. Jiménez-Pérez ZE, Singh P, Kim YJ, Mathiyalagan R, Kim DH, Lee MH, Yang DC. Applications of Panax ginseng leaves-mediated gold nanoparticles in cosmetics relation to antioxidant, moisture retention, and whitening effect on B16BL6 cells. J Ginseng Res. 2018; 42(3):327-333. https://doi.org/10.1016/j.jgr.2017.04.003.
- 13.Khan S, Ansari AA, Khan AA, Abdulla M, Al-Obeed O, Ahmad R. In vitro evaluation of anticancer and biological activities of synthesized manganese oxide nanoparticles. Med Chem Comm. 2016; 7(8): 1647-1653. https://doi.org/10.1039/C6MD00219F.
- 14. Alagarsamy A, Chandrasekaran S, Manikandan A. Green synthesis and characterization studies of biogenic zirconium oxide (ZrO<sub>2</sub>) nanoparticles for adsorptive removal of methylene blue dye. J Mol Struct. 2022; 1247:131275. https://doi.org/10.1016/j.molstruc.2021.131275.
- 15. Vijayakumar A, Chacko A, Jayaprakash P. Green synthesis of Mn<sub>3</sub>O<sub>4</sub> nanoparticles in zinc chloride: Urea: acetamide deep eutectic solvent-characterization, fluorescence sensing, antibacterial and antioxidant properties. J Mol Struct. 2025; 1321:139833. https://doi.org/10.1016/j.molstruc.2024.139833.
- 16.Sackey J, Akbari M, Morad R, Bashir AK, Ndiaye NM, Matinise N, Maaza M. Molecular dynamics and bio-synthesis of phoenix dactylifera mediated Mn<sub>3</sub>O<sub>4</sub> nanoparticles: Electrochemical application. J Alloys Compd. 2021; 854:156987. https://doi.org/10.1016/j.jallcom.2020.156987.
- 17. Shaik MR, Syed R, Adil SF, Kuniyil M, Khan M, Alqahtani MS, Shaik JP, Siddiqui MR, Al-Warthan A, Sharaf MA, Abdelgawad A. Mn<sub>3</sub>O<sub>4</sub> nanoparticles: Synthesis, characterization and their antimicrobial and anticancer activity against A549 and MCF-7 cell lines. Saudi J Biol Sci. 2021; 28(2):1196-1202. <a href="https://doi.org/10.1016/j.sjbs.2020.11.087">https://doi.org/10.1016/j.sjbs.2020.11.087</a>.
- 18. Van Tran T, Nguyen DT, Kumar PS, Din AT, Qazaq AS, Vo DV. Green synthesis of Mn<sub>3</sub>O<sub>4</sub> nanoparticles using Costus woodsonii flowers extract for effective removal of malachite green dye. Environ Res. 2022; 214(2):113925. https://doi.org/10.1016/j.envres.2022.113925.
- 19. Wang Y, Hou C, Lin X, Jiang H, Zhang C, Liu G. Dye degradation studies of hausmannite manganese oxide (Mn<sub>3</sub>O<sub>4</sub>) nanoparticles synthesized by chemical method. Appl Phys A. 2021; 127(4):277. https://doi.org/10.1007/s00339-021-04428-6.
- 20.Majeed AH, Mohammed LA, Hammoodi OG, Sehgal S, Alheety MA, Saxena KK, Dadoosh SA, Mohammed IK, Jasim MM, Salmaan NU. A review on polyaniline: Synthesis, properties, nanocomposites, and electrochemical applications. Int J Polym Sci. 2022; 2022(1):9047554. https://doi.org/10.1155/2022/9047554.
- 21.Mizban RJ, Jassim WH. The effect of nano sized TiO<sub>2</sub> particles on improving the stress resistance and thermal stability of unsaturated polyester. IHJPAS. 2025; 38(3):114-124. https://jih.uobaghdad.edu.iq/index.php/j/article/view/3949.
- 22.Ali AT, Ewies EF. Biosynthesis, characterization, adsorption and antimicrobial studies of zirconium oxide nanoparticles using punica granatum extract. IHJPAS. 2023; 36(4):262-673. <a href="https://doi.org/10.30526/36.4.3167">https://doi.org/10.30526/36.4.3167</a>.
- 23.Gabriela ÁM, Gabriela MD, Luis AM, Reinaldo PR, Michael HM, Rodolfo GP, Roberto VB. Biosynthesis of silver nanoparticles using mint leaf extract (Mentha piperita) and their antibacterial activity. Adv Sci Eng Med. 2017; 9(11):914-923. <a href="https://doi.org/10.1166/asem.2017.2076">https://doi.org/10.1166/asem.2017.2076</a>.
- 24.Shanan ZJ, Majed MD, Ali HM. Effect of the concentration of copper on the properties of copper sulfide nanostructure. Baghdad Sci J. 2022; 19(1):0225. https://doi.org/10.21123/bsj.2022.19.1.0225.

- 25.Khalil AS, Al-Shabander BM, Yaseen MH. Photocatalytic activity of tetragonal BaTiO<sub>3</sub> nanoparticles prepared by wet chemical method. In AIP Conference Proceedings 2021; 2372(1):130019. https://doi.org/10.1063/5.0066068.
- 26.Nassif II, Al-Shabander BM. Effects of MWCNTs on the tensile properties and thermal conductivity of BaTiO<sub>3</sub>/epoxy nanocomposites. Iraqi J Sci. 2020:2226-2231. https://doi.org/10.24996/ijs.2020.61.9.9.
- 27. Alrubaie HA, Alshabander BM. The effect of ZnO nanoparticles on the self-cleaning of ZnO/epoxy composites. In AIP Conference Proceedings 2022; 2437(1):020184. https://doi.org/10.1063/5.0094219.
- 28.AL-Janabi QAA, Hind Suhail Abdulhay. Effects of chronic exposure for imidacloprid and nano-imidacloprid on some biochemical and hematological parameters in male rats. IHJPAS 2025; 38(2): 23-30. https://jih.uobaghdad.edu.iq/index.php/j/article/view/3643.
- 29.Ruaa MD, Alsahib SA, Ascar IF. Synthesis, characterization and cyclazation of pyran using Ag<sub>2</sub>O nanoparticle from natural source "ginger". Iraqi J Agric Sci. 2021; 52(5):1171-1184. https://doi.org/10.36103/ijas.v52i5.1455.
- 30.Al-Bahadili ZR, Al-Hamdani AA, Rashid FA, Al-Zubaidi LA, Ibrahim SM. An evaluation of the activity of prepared zinc nanoparticles with extracted alfalfa plant in the treatment of heavy metals. Baghdad Sci J. 2022; 19(6 (Suppl.)):1399. <a href="https://doi.org/10.21123/bsj.2022.7313">https://doi.org/10.21123/bsj.2022.7313</a>.
- 31.Al-Saadi TM. Investigating the structural and magnetic properties of nickel oxide nanoparticles prepared by precipitation method. IHJPAS. 2022; 35(4):94-103. https://doi.org/10.30526/35.4.2872.
- 32.Al-Saadi TM, Kamil ZA. Study the effect of manganese ion doping on the size-strain of SnO<sub>2</sub> nanoparticles using X-ray diffraction data. IHJPAS. 2023; 36(3):158-166. https://doi.org/10.30526/36.3.3052.
- 33.Hadi DJ, Younus MA. Bio synthesis, characterization, and evaluation of the anticancer activity of gold and silver nanoparticles and their polyacetal nanocomposite. Iraqi J Sci. 2024; 65(12):6824-6841. https://doi.org/10.24996/ijs.2024.65.12.4.